Available online at www.sciencedirect.com

ScienceDirect

Ceramics International 40 (2014) 1951–1959

CERAMICS INTERNATIONAL

www.elsevier.com/locate/ceramint

Structurally enhanced photocatalytic activity of flower-like ZnO synthesized by PEG-assited hydrothermal route

Parag V. Adhyapak*, Satish P. Meshram, Dinesh P. Amalnerkar, Imtiaz S. Mulla*

Centre for Materials for Electronics Technology, Panchawati, Pashan Road, Pune-411008, India

Received 14 May 2013; received in revised form 20 July 2013; accepted 21 July 2013
Available online 27 July 2013

Abstract

Hierarchical nanostructured ZnO with uniform flower-like morphology was obtained by using PEG-assisted low-temperature (120°C) hydrothermal route. These structures are formed by systematic assembly of nanosheets (10–25 nm thick) with dominant {2-1-10} planes. The products were characterized by using X-ray diffraction (XRD), field emission scanning electron microscopy (FE-SEM), Raman and photoluminescence (PL) spectroscopy. These nanostructures display a strong structure-induced photocatalytic performance. It is observed that a significant improvement takes place in the photodegradation of methylene blue as compared with other morphologies such as; spheres, vesicular and nanosheets.

Keywords: Zinc oxide; Polyethylene glycol; Hydrothermal; Methylene blue; Photocatalytic activity

1. Introduction

ZnO is a wide band gap (3.37 eV) semiconductor with a large exciton binding energy (~60 meV). It has witnessed enormous interest because of advancement in synthesis and unique applications in various fields such as photocatalysis, solar cells, sensors, nanogenerators and optical waveguides [1–6]. Among these applications, the photocatalysis is a mostly studied one due to its high photosensitivity and stability [7,8]. It has been demonstrated that photocatalytic activity of ZnO nanostructures can be optimized by morphology control [9,10]. Therefore, considerable efforts have been devoted to develop convenient synthetic strategies for the synthesis of hierarchical ZnO structures. Accordingly, many types of ZnO nanostructures, such as nanowires, nanorod arrays, nanocombs, nanobelts, nanorings, nanocables etc. have been synthesized by various processes such as thermal evaporation deposition, template-mediated growth, metalorganic chemical vapor deposition (MOCVD) and carbothermic method [11–17]. However, most of these synthesis techniques require high temperature, vacuum or complicated controlling processes which limits the large scale production at low cost. Therefore, it is of great importance and necessity to develop inexpensive technique operating at mild reaction conditions. Hydrothermal method has proven to be a versatile approach for preparation of ZnO due to convenience and the simplicity in the operation.

Recently, there have been many reports on the preparation of ZnO nanostructures with variety of new morphologies. The growth of these differently shaped ZnO nanostructures largely depends on the relative stability of the growth and direction of crystal faces. Generally, the presence of capping agent capable of stabilizing a particular crystal facet by adsorption can alter the growth rate in different crystal planes [18,19]. In this context, several different templates/capping agents such as water-soluble polymers [20–22], various citrate salts [18,23,24], ethylene diamine [25], water-soluble diblock copolymers [26], surfactants [27–29] and amino acids [30] have been succefully used to tune the size and shape of ZnO nanostructures. In most of these methods of preparing hierarchical ZnO nanostructures, the externally added surfactants or capping agents were adsorbed preferentially on some crystal planes of the growing particles that ultimately alter the growth kinetics and relative stability

*Corresponding authors. Tel.: +91 020 25899273; fax: +91 020 25898180.
E-mail addresses: adhyapakp@yahoo.com (P.V. Adhyapak), ismulla2001@gmail.com (I.S. Mulla).

0272-8842/$ - see front matter © 2013 Elsevier Ltd and Techna Group S.r.l. All rights reserved.
http://dx.doi.org/10.1016/j.ceramint.2013.07.104

of the crystal faces and hence either promote or inhibit crystal growth in some particular crystal planes, resulting in the formation of anisotropic ZnO nanostructures. These studies showed good control over the morphology of ZnO; however, most of the organic additives used in these methods were expensive long chain molecules. Formation of metal oxide in the presence of a non ionic surfactant – polyethylene glycol (PEG) is well documented in the literature [31–33]. PEG due to its uniform and ordered chain structure is easily adsorbed at the surface of metal oxide colloid, which in turn reduces the surface activity. As the colloid adsorbs the polymer on some area of its surface, the growth rate of colloid in certain direction gets confined. Thus one can assume that the addition of PEG in metal oxide colloid modifies the growth kinetics, which finally leads to the anisotropic growth of crystals [34,35].

On the basis of above considerations, the present work developed a facile and environment friendly low-temperature hydrothermal route for large scale synthesis of flower-like ZnO structures using PEG as a capping agent. The as-prepared ZnO structures are composed of many nanosheets having thickness ~10–25 nm. Such structures are expected to have a high surface to volume ratio and stability against aggregation. As expected, synthesized flower-like ZnO exhibits a strong morphology induced photocatalytic activity towards photodegradation of methylene blue (MB) compared to their monomorphological ZnO powders of nanoparticles and nanosheets. The present work not only gives insight into understanding the growth behavior of complex ZnO nanostructures during hydrothermal synthesis but also sheds some light on the improvement of the photocatalytic performance by designing the assembly of materials.

2. Experimental

2.1. Chemicals

All the reagents used in the present investigation were of analytical grade and used without further purification. Zinc nitrate hexahydrate, zinc acetate, poly ethylene glycol (PEG-400) and sodium hydroxide were purchased from Merk (India). Methylene Blue was purchased from SdFine Chemical Co. Double distilled water was used for preparation of all experimental solutions.

2.2. Preparation of flower-like ZnO

In a typical procedure to synthesize flower-like ZnO, zinc nitrate hexahydrate $Zn(NO_3)_2 \cdot 6H_2O$, 0.1 g (0.3 mmol) was dissolved in 20 ml PEG. To this well mixed solution, sodium hydroxide (NaOH, 0.24 g (6 mmol) dissolved in 20 ml H_2O and 30 ml Ethanol) solution was dropwise added. The mixed solution was sonicated for 15 min on ultrasonic bath and then hydrothermally treated at 120 °C for 12 h, and then allowed to cool to room temperature naturally. The final white precipitate was separated by centrifuge, washed with distilled water and absolute ethanol several times to remove the possible residues and then dried at 60 °C for 12 h.

2.3. Characterization

The phase identification of the nanostructured ZnO powders was done by X-ray diffraction (XRD) using a Rigaku Miniflex X-ray diffractometer with CuKα irradiation at λ=1.5406 Å. The surface morphology was investigated by Field Emission Scanning Electron Microscope (FE-SEM) JEOL-JSM Model 6700 F field emission scanning electron microscope. The photoluminescence spectra of aqueous suspension of ZnO were recorded on F-2500 Fluorescence spectrophotometer. For PL measurement, the samples' water suspensions were excited at the wavelength of 340 nm. UV–visible absorption spectra of an aqueous suspension of ZnO products were recorded on JASCO V-570 spectrophotometer by transferring an appropriate volume of ZnO suspension to quartz cuvette. The spectral changes in concentration of MB during photocatalytic degradation were also studied using the same spectrophotometer. FTIR spectra of as-prepared purified ZnO powders were recorded using KBr pellets on a Perkin-Elmer 1090 spectrometer.

2.4. Photocatalytic activity measurements

The photocatalytic activity experiments on the as-prepared ZnO products for the degradation of MB were performed at ambient temperature. A Pyrex beaker (250 mL) was used as the photoreactor. ZnO products as catalyst (50 mg) were added in the aqueous methylene blue solution ($C_{16}H_{18}ClN_3S_3 \cdot 3H_2O$) ($5.0 \times 10^{-5}$ M, 100 mL), and the solution was magnetically stirred in the dark for 1 h to reach the adsorption equilibrium of MB with the catalyst and then exposed to sunlight. At given irradiation time intervals, a series of aqueous solutions in a certain volume were collected and centrifuged to remove the catalysts and were then analyzed by a spectrophotometer. The concentration of methylene blue was determined by monitoring the changes in the main absorbance centered at 663 nm.

3. Results and discussion

3.1. Morphology and structure

The morphologies and phases of as-synthesized ZnO were examined by using FE-SEM and XRD techniques. Fig. 1 shows FE-SEM and XRD patterns of as-prepared ZnO product. The morphology (Fig. 1a) shows systematic emergence of well-defined three dimensional (3D) flower-like ZnO structures having diameters in the range of 1–2 μm. A magnified FE-SEM image presented in Fig. 1b shows that the flower-like structures are assembled by many densely arranged nanosheets as “petals”. A close-up view of the nanosheets-built flowers in Fig. 1c reveals that these nanosheets have thickness of 10–25 nm and are grown upward from center to form many groves. Such 3D nanostructures can have the ability to improve the chemical properties or serve as transport paths for small molecules. Fig. 1d shows the XRD pattern of as-synthesized flower-like ZnO sample. The diffraction peaks at 2θ=31.8, 34.5, 36.4, 47.5, 57.1, 63.2, 66.7, 67.8, 69, 72.6,

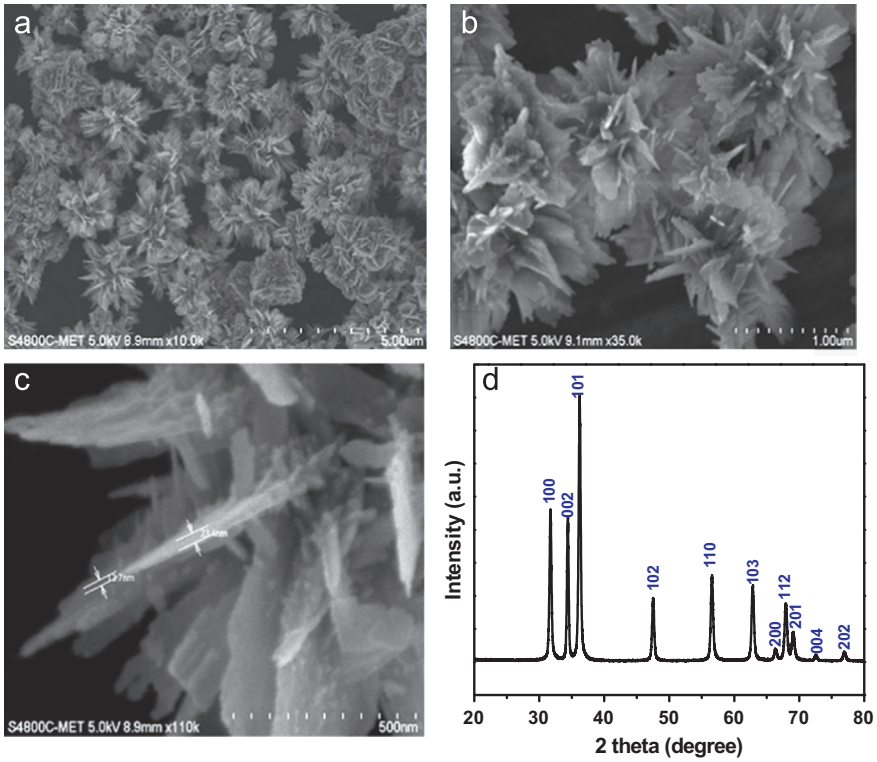

Fig. 1. FE-SEM images and XRD pattern of ZnO prepared by hydrothermal route with PEG and 0.3 mmol $Zn(NO_3)_2$ and 6.0 mmol of NaOH at 120 °C for 12 h: (a–c) FE-SEM image; (d) XRD pattern.

and 76.8° match with the wurtzite hexagonal ZnO having lattice constants of *a* and *c* equal to 3.25 and 5.21 Å, respectively (JCPDS file no. 36-1451). It may be noted that no peak corresponding to impurities, such as zinc hydroxide was observed in the XRD pattern indicating formation of pristine ZnO. Moreover, comparatively more intense peak for the (101) plane suggests the anisotropic growth of the zinc oxide material.

The as-synthesized flower-like ZnO was further characterized by using photoluminescence spectroscopy. The PL spectrum of ZnO consists of three emission bands, a near-band-edge (UV) emission and two broad deep-level (visible) emissions. The visible emission is usually considered to be related to various intrinsic defects produced during preparation and post treatment. Normally these defects are located on the surface of ZnO structure. Fig. 2 presents PL spectrum of as-synthesized flower-like ZnO product excited at 225 nm UV light from a He–Cd laser. It shows a UV emission peak at 395 nm (~3.13 eV) and a green emission peak at 460 nm (~2.69 eV). The emission at 395 nm corresponds to the near band-edge emission resulting from recombination of free excitons whereas a weak emission peak at 460 nm can be attributed to electron transition mediated by defect levels in band gap. It may be noted that the usually observed defect related to deep level emissions were nearly missing in our sample, indicating formation of high optical quality ZnO.

Raman spectroscopy is performed to study the degree of crystallization of as-synthesized flower-like ZnO. Fig. 3 shows Raman spectra of ZnO sample in the range of 200–800 nm.

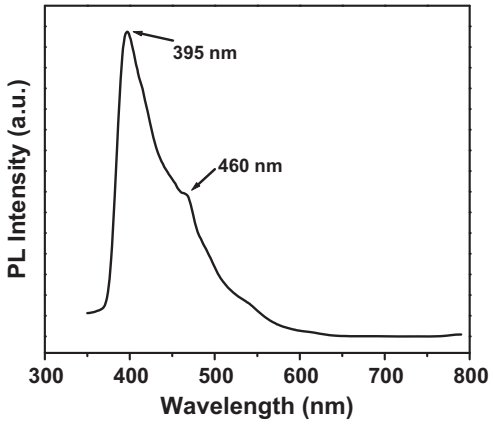

Fig. 2. PL spectrum of ZnO product prepared by hydrothermal route with 0.3 mmol $Zn(NO_3)_2$ and 6.0 mmol of NaOH at 120 °C for 12 h.

ZnO with wurtzite structure belongs to the C6V 4 space group. At the Γ point of Brillouin zone, optical phonons have the following irreducible representation: Γ_{opt}=A1+2B1+E1+2E2 [36]. Among these, A1 and E1 modes are polar and can be split into transverse (TO) and longitudinal optical (LO) components, with all being Raman and infrared active. For the as-synthesized flower-like ZnO the vibration peaks can be clearly observed at 203, 332, 436, 548, and 707 cm^{-1} (Fig. 3). Among these peaks, the strongest one, centered at about 436 cm^{-1} is characteristic of the high-frequency E2 mode of wurtzite structure. The peak at 548 cm^{-1} corresponds to LO phonon of A1 and E1, respectively. Besides these "classical"

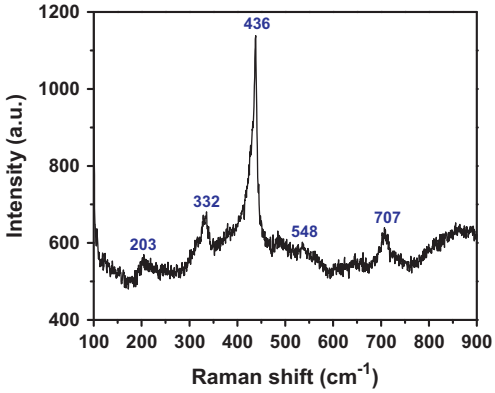

Fig. 3. Raman spectrum of ZnO prepared by hydrothermal route with 0.3 mmol $Zn(NO_3)_2$ and 6.0 mmol of NaOH at 120 °C for 12 h.

Raman modes, the Raman spectrum also shows other modes with frequencies of 203, 332, and 707 cm^{-1}. These additional peaks cannot be explained within the framework of bulk single phonon modes and are attributed to the multiphonon scattering processes [37].

3.2. Formation of flower-like ZnO

As a polar crystal, ZnO structure consists of hexagonally close-packed oxygen and zinc atoms. It has several main crystal planes, top tetrahedron corner-exposed polar zinc (0001) plane, six symmetric nonpolar {10–10} planes parallel to the [0001] direction, and a basal polar oxygen (000–1) plane. Normally, for ZnO, the highest surface energy of the (0001) plane promotes the growth along *c*-axis, and results in the familiar 1D nanostructures (nanowires, nanorods, and nanotubes) in which the relative surface area of the {0001} plane is very low. In our present case, the flower-like ZnO structures have been demonstrated to be able to fabricate by a simple surfactant (PEG)-assisted hydrothermal route. It may be noted that the 3-D ZnO architectures are organized by the 2-D nanosheets, which are different from some previous studies mainly focused on nanorods as the nanobuilding blocks [38,39].

A series of experiments were performed to understand formation of hierarchical flower-like ZnO. To find the role of PEG on morphology of ZnO nanostructures we performed the experiment in absence of PEG while keeping all other experimental conditions unchanged. Fig. 4a displays FE-SEM image of ZnO prepared without PEG. These are irregular small sheet-like structures having length in the range of 0.2–0.5 μm show tendency to cling together in irregular manner, which suggests significant role of PEG as an assembling agent. The inset of Fig. 4a shows corresponding XRD pattern of this ZnO exhibiting preferential growth orientation along the [0001] plane. The close observation of XRD spectrum of ZnO synthesized with and without PEG indicates that the amount of PEG has influence on the preferential growth orientation of ZnO. As shown in Fig. 4b the intensity ratio of (10–10)/(0002) evidently decreases for the sample prepared without PEG, which is 1.24 for flower-like ZnO nanostructures and reduced to 1.18 for the irregularly shaped ZnO prepared without PEG. These FE-SEM and XRD results illustrate significant effect of PEG on the morphology and crystal orientation. As evident, the growth habit of crystals is related to the growth rate of various crystal faces bounding the crystal, which is affected by intrinsic crystal structure and external conditions including the kinetic energy barrier, temperature, time and capping molecules and so on. PEG is known to be an important capping molecule which can bind to the positively charged Zn^{2+} terminated (0001) polar plane more strongly than to other nonpolar surfaces due to coulombic force. Such anisotropy would certainly slow down crystal growth along [0001] direction. From the kinetic viewpoint the fastest growing planes will disappear to leave behind the slowest growing planes as the crystal facets. Thus, it is comprehensible that along with the use of PEG, the orientation of ZnO product has changed from (0001) to (10–10). Accordingly, the morphology has shaped into nanosheets built microflowers.

In addition to this, experiments were carried out to study influences of concentrations of Zn^{2+} and OH^- on morphology of ZnO. Fig. 5(a,b) shows FE-SEM image of ZnO sample obtained from the reaction of 0.6 mmol $Zn(NO_3)_2$ and 3 mmol of NaOH, with other experimental conditions unchanged. It can be seen from the figure that the ZnO consists of vesicles with rough surfaces. Whereas, the reaction carried out with 0.15 mmol of $Zn(NO_3)_2$ and 6 mmol of NaOH yielded nonuniform nanosheets having lengths in the range 200–500 nm (Fig. 5c,d). These results indicate that the concentrations of Zn^{2+} and OH^- are the key parameters for formation of well-shaped flower-like ZnO structures. Moreover, to study the effect of zinc source on morphology of ZnO, another experiment with zinc acetate as a starting material was carried out. Fig. 5(e,f) represents morpholgy of as-obtained product. It can be seen from figure that the use of zinc acetate instead of zinc nitrate significantly affects the flower-like morphology and results into formation of oval/spherical nest-like product.

Finally, in order to understand the formation of ZnO microflowers, a time dependent morphology evolution was examined by FE-SEM. Fig. 6 shows FE-SEM images of samples obtained at different reaction stages (3 h, 6 h and 9 h) of hydrothermal process. As shown in Fig. 6a, the 3 h reaction resulted in undeveloped part of flower-like ZnO which consists of some loose nanosheets with tiny nanoparticles on their surfaces, which might serve as the growing units for other nanosheets. Fig. 6b is the FE-SEM view of sample collected after 6 h of reaction; it shows co-existence of nanosheets and flower-like structures. The sample obtained after 9 h reaction (Fig. 6c) is composed of nearly flower-like ZnO nanostructure with larger size at the expense of nanosheets. As the reaction proceeds, eventually no nanosheets existed and the sample is composed of perfect flower-like 3D nanostructure. The morphology and size of ZnO remains unchanged even after 12 h of hydrothermal treatment (Fig. 6d). This tends to suggest that the process begins with formation of large number of nanosheets with their (0001) surface capped by PEG, further; the nanosheets undergo systematic attachment resulting into the formation of hierarchical ZnO nanostructure.

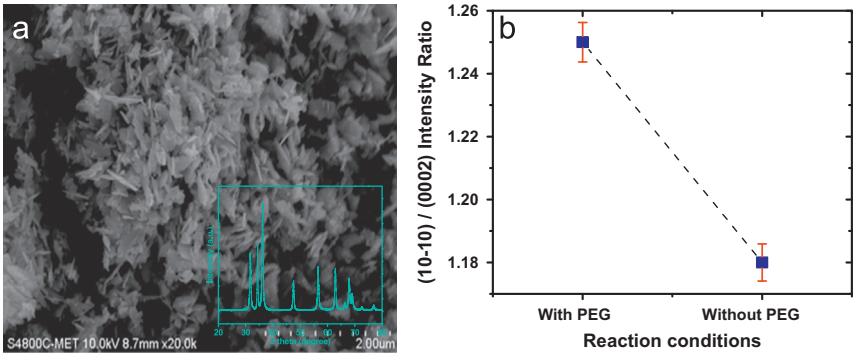

Fig. 4. (a) FE-SEM image of ZnO prepared by hydrothermal route without PEG using 0.3 mmol $Zn(NO_3)_2$ and 6.0 mmol of NaOH at 120 °C for 12 h (corresponding XRD pattern in the inset); (b) Plot of the (10–10)/(0002) intensity ratio for the samples prepared with and without PEG.

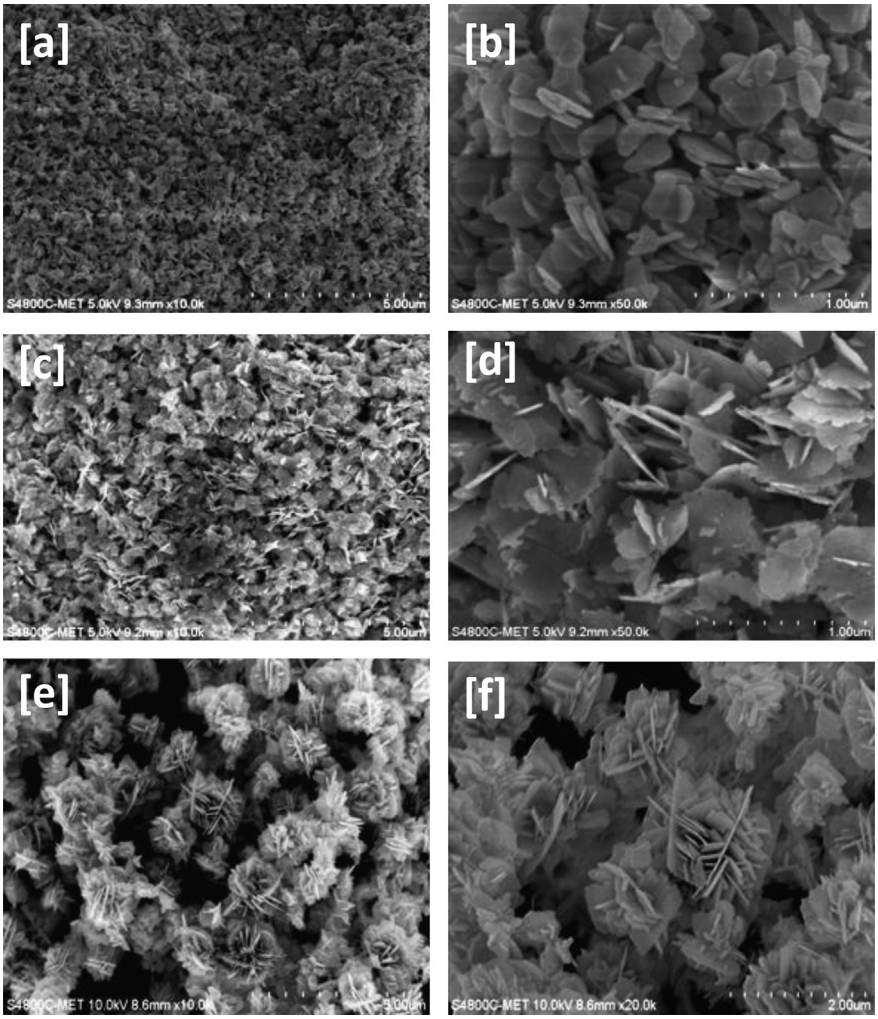

Fig. 5. (a) FE-SEM images of ZnO prepared by PEG assisted hydrothermal route using different amounts of $Zn(NO_3)_2$ and NaOH: (a) 0.6 mmol of $Zn(NO_3)_2$ and 2.0 mmol of NaOH (b) 0.15 mmol of $Zn(NO_3)_2$ and 6.0 mmol of NaOH. (c,d) FE-SEM image of the product prepared with $Zn(OAc)_2$ instead of $Zn(NO_3)_2$ at 120 °C for 12 h (6.0 mmol of NaOH).

Based on the above discussion, possible growth mechanism for the formation of flower-like ZnO can be explained by considering the wurtzite structure of ZnO. ZnO has a hexagonal wurtzite structure consisting of planes of tetrahedrally coordinated O^{2-} and Zn^{2+} ions, mounted alternately along the polar *c*-axis. The well developed crystal faces of ZnO evince positively charged polar (0001)-Zn surfaces, six symmetric nonpolar $(1\bar{0}10)$ planes of the side facets and negatively charged $(00\bar{0}1)$-O polar surfaces [38]. The crystal growth rate in different directions generally follows the order $[0001] > [1\bar{0}10] \geq [1\bar{0}\bar{1}1] > [1\bar{0}11] > [00\bar{0}1]$ [39]. During

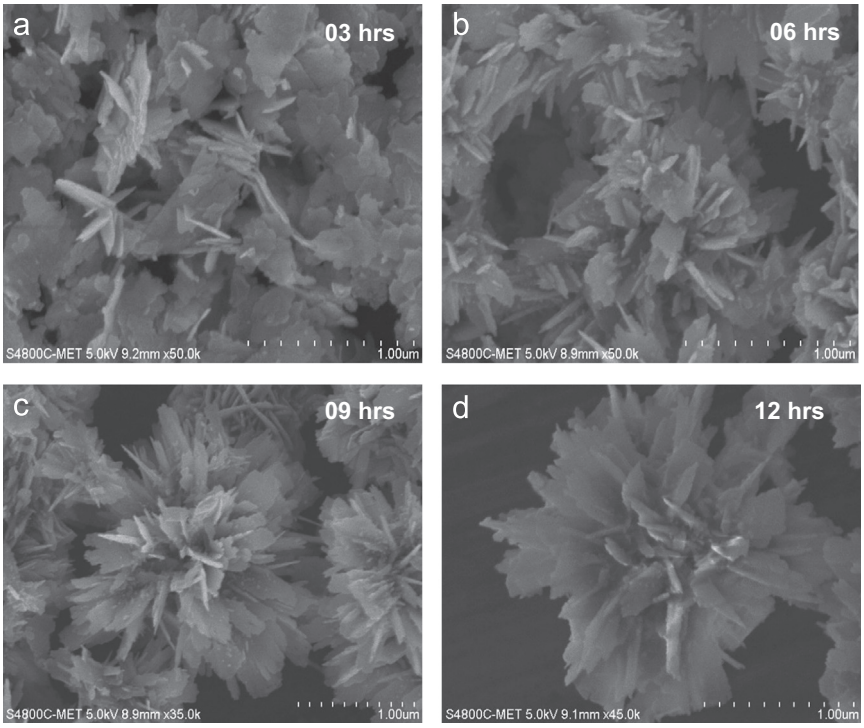

Fig. 6. (a) FE-SEM images of ZnO obtained after different reaction time at 120 °C in PEG assisted hydrothermal reaction with 0.3 mmol of $Zn(NO_3)_2$ and 6.0 mmol of NaOH: (a) 3 h, (b) 6 h, (c) 9 h and (d) 12 h.

the course of reaction, zinc acetate produces Zn^{2+} cation which readily reacts with OH^- anions forming the basic growth unit $[Zn(OH)_4]^{2-}$. These $[Zn(OH)_4]^{2-}$ ions then decompose to generate ZnO molecular species according to following reactions.

$$Zn^{2+} + OH^- \rightarrow [Zn(OH)_4]^{2-} \quad (1)$$

$$[Zn(OH)_4]^{2-} \rightarrow ZnO + H_2O + 2OH^- \quad (2)$$

Addition of NaOH solution results into a white precipitate of insoluble $Zn(OH)_2$ which later becomes a clear solution of $[Zn(OH)_4]^{2-}$. Increasing the OH- content helps to make solution clearer and ease the formation of ZnO [40]. Cheon et al. have reported that there are four different parameters, kinetic energy barrier, temperature, time and capping molecules that can influence the growth pattern of nanocrystals under nonequillibrium kinetic growth conditions in the solution based approach [41,42]. For the formation of flower type ZnO architecture, it seems that as the reaction proceeds, the surfaces whose normal directions are of fast growth rate disappear while the slow growing surfaces remain. We believe that during the PEG assisted hydrothermal synthesis, the capping agent (PEG) plays an important role in the formation of the observed hierarchical nanostructures. During synthesis, PEG molecules are preferably adsorbed on the positive polar plane {0001} by competing with growth units, which minimizes the anisotropic growth of ZnO along {0001} direction. However, there exist inevitable defects or bulges on the lateral planes of the initially formed ZnO crystals. Such bulges will preferentially grow along the $(0\bar{1}10)$ direction with lagging {0001} direction within the $(\bar{2}\bar{1}10)$ plane resulting into formation of nanosheets on the lateral surface. Moreover, there also exist some outshoots on the growing nanosheets which grow and lead to the formation of secondary branched nanosheets with terminated $(\bar{2}\bar{1}10)$ facets and interplaner angles ~60°. As the hydrothermal reaction time proceeds, third or fourth branched nanosheets could be formed on the as-grown nanosheets resulting into formation of flower-like ZnO architecture. The overall schematic illustration of the formation of flower-like nanostructure is depicted in Fig. 7.

3.3. Photocatalytic activity

It is well established that ZnO has been used as a semiconductor photocatalyst for the photoreductive dehalogenation of halogenated phenol/benzene derivatives and the photocatalytic degradation of organic compounds. Obviously, the as-synthesized ZnO nanoarchitectures reported here should show a higher photocatalytic activity because of its special structure. A proof-of-concept demonstration of the structure-induced enhancement of photocatalytic performance of flower-like ZnO was carried by sunlight-mediated degradation of a well known Methylene Blue (MB) dye. Fig. 8 shows the UV–visible spectra changes of a MB dye aqueous solution (initial concentration: 5.0×10^{-5} M, 100 mL) with 50 mg of the as-prepared flower-like ZnO powder under sunlight irradiation for different durations. The main absorption peak centered at 664 nm corresponding to MB molecules, decreases rapidly with extension of irradiation time and completely disappears after 70 min. Further exposure leads to no absorption peak in the whole spectrum indicating the total decomposition of MB dye.

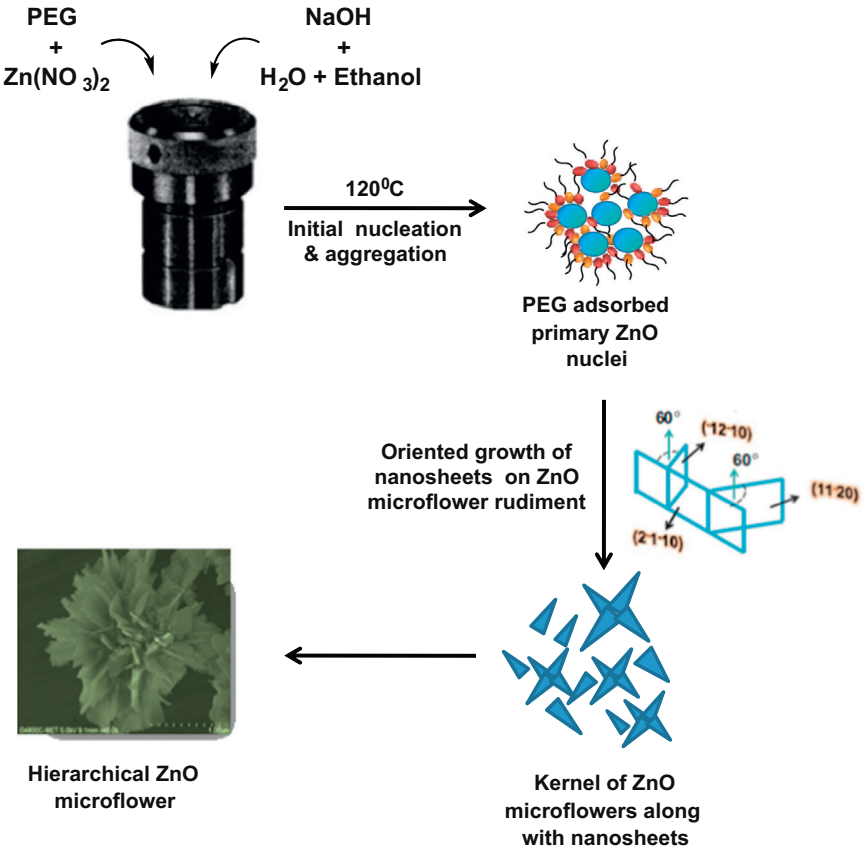

Fig. 7. Schematic illustration of formation of hierarchical flower-like ZnO nanostructures.

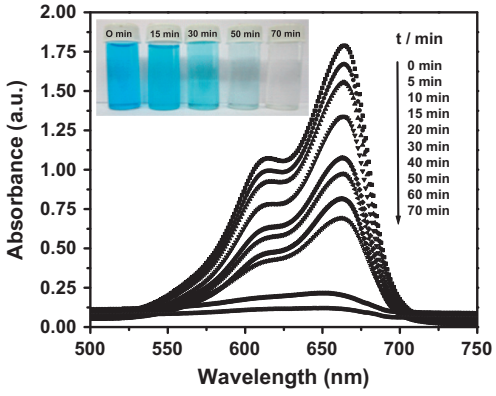

Fig. 8. Time dependent optical absorption spectra changes of MB dye aqueous solution (initial concentration: 5.0×10^{-5} M, 100 mL) in presenscence of flower-like ZnO (50 mg) under sunlight irradiation and corresponding color changes in initial solution at 15, 30, 50 and 70 mins of photodegradation reaction.

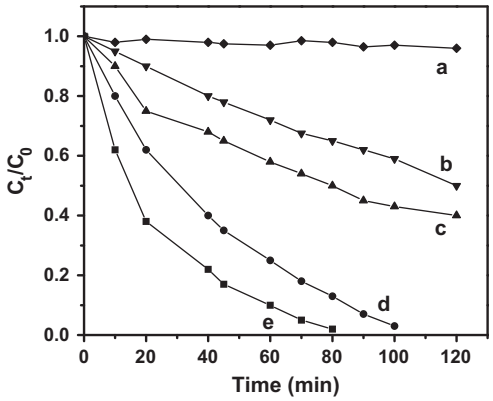

Fig. 9. Plot of the MB normalized concentration (from the optical absorbance measurements at 664 nm) in the solution (100 mL) with different catalysts (50 mg) versus irradiation time. Initial MB concentration: 5×10^{-5} M. (a) without any catalyst (b) sheet-like ZnO (c) spherical ZnO (d) nest-like ZnO and (e) flower-like ZnO.

A series of color changes in the sample is shown in inset of Fig. 8, corresponding to the sequential changes of absorption measurements at initial, 15, 30, 50 and 70 min of reaction. It makes clear that the intense blue color of starting solution gradually disappears with increasing sunlight irradiation time. Further to demonstrate the structure-induced enhancement of photocatalytic performance of flower-like ZnO, experiments were performed using other nanostructured ZnO powders (vesicular, sheet-like and nest-like). A controlled experiment without use of any catalyst, keeping all other parameters unchanged, was also performed. The results are shown in Fig. 9, which corresponds to normalized concentrations of MB solution versus irradiation time from the optical absorbance measurements at 664 nm. In absence of any catalyst only a slow and negligible decrease in the concentration of MB was detected (curve a, Fig. 9). The addition of catalysts leads to a significant degradation of MB which is also seen to be dependent on the

morphology. The activity increases in turn for the nanostructured ZnO powders: sheet-like (curve b), vesicular (curve c), nest-like (curve d) and flower-like (curve e). Flower-like ZnO possesses a highest catalytic activity compared to its other counterparts and degraded the MB dye aqueous solution to 98% after 70 min of sunlight irradiation. In addition to this, to evaluate the durability of photocatalytic activity, experiments were carried by re-using the catalyst in fresh MB solution under sunlight irradiation. Fig. 10 shows photodegradation results for three consecutive cycles using vesicular, sheet-like, nest-like and flower-like ZnO nanostructures. The figure clearly indicates that flower-like ZnO exhibits best durability even after the third cycle and is more stable compared to other ZnO nanostructures.

The photocatalytic superiority of flower-like ZnO over the other nanostructured ZnO can be attributed to their special structural features. In terms of the well explored mechanism for photocatalytic degradation of organic dye, which occurs by an indirect pathway involving hydroxyl radicals as the oxidizing intermediate as flows:

$$ZnO + h\upsilon \rightarrow ZnO(e_{CB}^{-} + h_{VB}^{+}) \quad (3)$$

$$H_2O + h_{VB}^{+} \rightarrow H^{+} + OH \quad (4)$$

$$\text{Dye molecule} + OH \rightarrow \text{Oxidation products} \quad (5)$$

Under sunlight irradiation, the conduction band electrons (e_{CB}^{-}) and valence-band holes (h_{VB}^{+}) are generated on the surface of ZnO. The holes can react with water adhering to surfaces of ZnO to form highly reactive hydroxyl radicals (OH) which are responsible for degradation of organic dye. The origins of photocatalytic superiority of flower-like ZnO nanostructures can be attributed to the presence of numerous nanosheets generating a large specific area. The individual component and nanosheets built large interspaces leading to the enhancement in MB dye adsorption, transportation and light harvesting. In addition to this, the nanosheets of flower-like ZnO have very small thickness of 10–25 nm which is close to the regime where quantum size effect is prominent. The size quantized nanosheets would promote the charge-transfer in the materials. The increase in charge transfer rates drastically reduces the direct recombination of the photogenerated electron/hole pairs [43], which is essential to enhance the photocatalytic efficiency in the degradation of dye molecule. Thus, as stated above, excellent photocatalytic performance of flower-like ZnO along with competitive photoactivity of nest-like ZnO nanostructures is obtained. In comparison, the ZnO having sheet-like and vesicular morphology lacks the above-mentioned structural advantage and thus probably have inferior photocatalytic activity in photodegradation of MB dye. A more detailed understanding of the photocatalytic activity of flower-like ZnO nanostructures is in progress.

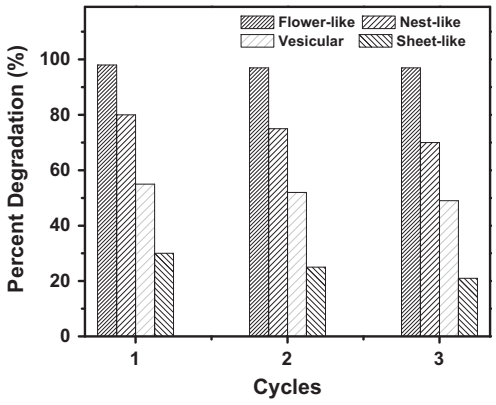

Fig. 10. Comparision of photodegradation performance within three cycles (1: Original, 2: first recycled, 3: second recycled) for different ZnO catalysts.

4. Conclusion

In summary, a novel hierarchical flower-like ZnO nanostructures built by nanosheets has been synthesized at large scale through a simple and economical PEG assisted hydrothermal method. The nanosheets have a very small thickness in the range of 10–25 nm. These ultrathin nanosheets interlace each other and assemble into the flower-like ZnO nanostructures. The flower-like ZnO demonstrates strong structurally enhanced photocatalytic activity as compared with the other nanostructured ZnO having nest-like, sheet-like and vesicular morphology. These hierarchical ZnO flowers are also expected to be useful for other applications such as dye-sensitized solar cells and gas sensing. Moreover, the present work further hints that this facile route can be easily extended to synthesize other metal-oxides with novel and hierarchical nanostructure.

Acknowledgment

I. S. Mulla gratefully acknowledges CSIR, New Delhi, India for awarding him Emeritus Scientist Scheme.

References

[1] F. Lu, W. Cai, Y. Zhang, ZnO hierarchical micro/nanoarchitectures: solvothermal synthesis and structurally enhanced photocatalytic performance, Advanced Functional Materials 18 (2008) 1047–1056.
[2] M. Law, L. Greene, J.C. Johnson, R. Saykally, P. Yang, Nanowire dye-sensitized solar cells, Nature Materials 4 (2005) 455–459.
[3] Y. Zeng, T. Zhang, L. Wang, R. Wang, W. Fu, H. Yang, Synthesis and ethanol sensing properties of self-assembled monocrystalline ZnO nanorod bundles by poly(ethylene glycol)-assisted hydrothermal process, Journal of Physical Chemistry C 113 (2009) 3442–3448.
[4] Z.L. Wang, J. Song, Piezoelectric nanogenerators based on zinc oxide nanowire arrays, Science 312 (2006) 242–246.
[5] M.H. Huang, S. Mao, H. Feick, H. Yan, Y. Wu, H. Kind, E. Weber, R. Russo, P. Yang, Room-temperature ultraviolet nanowire nanolasers, Science 292 (2001) 1897–1899.
[6] L. Cao, B. Zou, A. Pan, S. Xie, D. Liu, X. Zhu, Room temperature green light waveguide behavior of micron-sized single-crystalline ZnO rods, Physics of Low-Dimensional Structures 1 (2006) 36–40.
[7] E.S. Jang, J.H. Won, S.-J. Hwang, J.-H. Choy, Fine tuning of the face orientation of ZnO crystals to optimize their photocatalytic activity, Advanced Materials 18 (2006) 3309–3312.
[8] Y. Liu, Z.H. Kang, Z.H. Chen, I. Shafiq, J.A. Zapien, I. Bello, W.J. Zhang, S.T. Lee, Synthesis, characterization, and photocatalytic application of different ZnO nanostructures in array configurations, Crystal Growth and Design 9 (2009) 3222–3227.

[9] M.R. Hoffmann, S.T. Martin, W. Choi, D.W. Bahnemann, Environmental applications of semiconductor photocatalysis, Chemical Reviews 95 (1995) 69–96.
[10] E.S. Jang, J.H. Won, S.J. Hwang, J.H. Choy, Fine tuning of the face orientation of ZnO crystals to optimize their photocatalytic activity, Advanced Materials 18 (2006) 3309–3312.
[11] B. Xiang, P. Wang, X. Zhang, S.A. Dayeh, D.P.R. Aplin, C. Soci, D. Yu, D. Wang, Rational synthesis of p-type zinc oxide nanowire arrays using simple chemical vapor deposition, Nano Letters 7 (2007) 323–328.
[12] C. Geng, Y. Jiang, Y. Yao, X. Meng, J.A. Zapien, C.S. Lee, Y. Lifshitz, S.T. Lee, Well-aligned ZnO nanowire arrays fabricated on silicon substrates, Advanced Functional Materials 14 (2004) 589–594.
[13] C.S. Lao, P.X. Gao, R.S. Yang, Y. Zhang, Y. Dai, Z.L. Wang, Formation of double-side teethed nanocombs of ZnO and self-catalysis of Zn-terminated polar surface, Chemical Physics Letters 417 (2006) 358–362.
[14] Z.W. Pan, Z.R. Dai, Z.L. Wang, Nanobelts of semiconducting oxides, Science 291 (2001) 1947–1949.
[15] X.Y. Kong, Y. Ding, R. Yang, Z.L. Wang, Single-crystal nanorings formed by epitaxial self-coiling of polar nanobelts, Science 303 (2004) 1348–1351.
[16] J. He, Y.H. Huang, Y. Zhang, Y.S. Gu, Z. Ji, C. Zhou, Large-scale synthesis, microstructure and growth mechanism of self-assembled core–shell ZnO/SiOx nanowires, Materials Letters 60 (2006) 150–153.
[17] Z.L. Wang, Nanostructures of zinc oxide, Materials Today 7 (2004) 26–33.
[18] T.L. Sounart, J. Liu, J.A. Voigt, M. Huo, E.D. Spoerke, B. Mckenzie, Secondary nucleation and growth of ZnO, Journal of the American Chemical Society 129 (2007) 15786–15793.
[19] Z.R. Tian, J.A. Voigt, J. Liu, B. Mckenzie, M.J. Mcdermott, Biomimetic arrays of orientied helical ZnO nanorods and columns, Journal of the American Chemical Society 124 (2002) 12954–12955.
[20] R. Muoz-Espi, G. Jeschke, I. Lieberwirth, C.M. Gmez, G. Wegner, ZnO – latex hybrids obtained by polymer-controlled crystallization: a spectroscopic investigation, Journal of Physical Chemistry B 111 (2007) 697–707.
[21] H. Zhang, D. Yang, D. Li, X. Ma, S. Li, D. Que, Controllable growth of ZnO microcrystals by capping molecule assisted hydrothermal process, Crystal Growth and Design 5 (2005) 547–550.
[22] M.H. Rashid, M. Raula, R.R. Bhattacharjee, T.K. Mandal, Low-temperature polymer-assisted synthesis of shape tunable zinc oxide nanostructures dispersible in both aqueous and non-aqueous media, Journal of Colloid and Interface Science 339 (2009) 249–258.
[23] Z.R. Tian, J.A. Voigt, J. Liu, B. Mckenzie, M.J. Mcdermott, M.A. Rodriguez, H. Konishi, H. Xu, Complex and oriented ZnO nanostructures, Nature Materials 2 (2003) 821–826.
[24] S. Cho, J. Jung, S. Jung, B.R. Lee, E. Oh, K. Lee, Precursors effects of citric acid and citrates on ZnO crystal formation, Langmuir 25 (2009) 3825–3831.
[25] U. Pal, P. Santiago, Controlling the morphology of ZnO nanostructures in a low-temperature hydrothermal process, Journal of Physical Chemistry B 109 (2005) 15317–15321.
[26] A. Taubert, G. Glasser, D. Palms, Kinetics and particle formation mechanism of Zinc oxide particles in polymer-controlled precipitation from aqueous solution, Langmuir 18 (2002) 4488–4494.
[27] J. Du, Z. Liu, Y. Huang, Y. Gao, B. Han, W. Li, G. Yang, Controll of ZnO morphologies via surfactant assisted route in the subcritical water, Journal of Crystal Growth 280 (2005) 126–134.
[28] L Guo, Y.L. Ji, H. Xu, P. Simon, Z. Wu, Regularly shaped, single crystalline ZnO nanorods with wurzite structure, Journal of the American Chemical Society 124 (2002) 14864–14865.
[29] X.L. Zhang, R. Qiao, R. Qiu, J.C. Kim, Y.S. Kang, Fabrication of hierarchical ZnO nanostructures via a surfactant-directed process, Crystal Growth and Design 9 (2009) 2906–2910.
[30] M. Umetsu, M. Mizuta, K. Tsumoto, S. Ohara, S. Takami, H. Watanabe, I. Kumagai, T. Adschiri, Bioassisted room-temperature immobilization and mineralization of zinc oxide—the structural ordering of zno nanoparticles into a flower-type morphology, Advanced Materials 17 (2005) 2571–2575.
[31] J. Duan, X. Huang, E. Wang, EG-assisted synthesis of ZnO nanotubes, Materials Letters 60 (2006) 1918–1921.
[32] T. Thongtem, S. Jattukul, A. Phuruangrat, S. Thongtem, The effect of H_2O and PEG on the morphologies of ZnO nanostructures synthesized under microwave radiation, Journal of Alloys and Compounds 491 (2010) 654–657.
[33] Z. Zhu, D. Yang, H. Liu, Microwave-assisted hydrothermal synthesis of ZnO rod-assembled microspheres and their photocatalytic performances, Advanced Powder Technology 22 (2011) 493–497.
[34] H. Zhang, D. Yang, X. Ma, N. Du, J. Wu, D. Que, Straight and thin ZnO nanorods: hectogram-scale synthesis at low temperature and cathodoluminescence, Journal of Physical Chemistry B 110 (2006) 827–830.
[35] Y. Zeng, T. Zhang, W. Fu, Q. Yu, G. Wang, Y. Zhang, Y. Sui, L. Wang, C. Shao, Y. Liu, H. Yang, G. Zou, Fabrication and optical properties of large-scale nutlike ZnO microcrystals via a low- temperature hydrothermal route, Journal of Physical Chemistry C 113 (2009) 8016–8022.
[36] F. Decremps, J.P Porres, A.M. Saitta, J.C. Chervin, A. Polian, High-pressure Raman spectroscopy study of wurtzite ZnO, Physical Review B 65 (2002) 092101.
[37] R.B. Liu, A.L. Pan, H.M. Fan, F.F. Wang, Z.X. Shen, G.Z. Yang, S. S. Xie, B.J. Zou, Phonon-assisted stimulated emission in Mn-doped ZnO nanowires, Physics: Condensed Matter 19 (2007) 136206.
[38] Y.H. Ni, J.S. Zhu, L. Zhang, J.M. Hong, Hierarchical ZnO micro/nanoarchitectures: hydrothermal preparation, characterization and application in the detection of hydrazine, Crystal Engineering Communication 12 (2010) 2213–2218.
[39] P. Jiang, J.J. Zhou, H.F. Fang, C.Y. Wang, Z.L. Wang, S.S. Xie, Hierarchically shelled ZnO structures made of bunched nanowire arrays, Advanced Functional Materials 17 (2007) 1303–1310.
[40] S. Komarneni, M. Bruno, E. Mariani, Synthesis of ZnO with and without microwaves, Materials Research Bulletin 35 (2000) 1843–1847.
[41] A. Wei, X.W. Sun, C.X. Xu, Z.L. Dong, Y. Yag, S.T. Tan, W. Huang, Growth mechanism of tubular ZnO formed in aqueous solution, Nanotechnology 17 (2006) 1740–1744.
[42] S.M. Lee, S.N. Cho, J. Cheon, Anisotropic shape control of colloidal inorganic nanocrystals, Advanced Materials 15 (2003) 441–444.
[43] C.H. Ye, Y. Bando, G.Z. Shen, D. Golberg, Thickness-dependent photocatalytic performance of zno nanoplatelets, Journal of Physical Chemistry B 110 (2006) 15146–15151.